



Self-adaptive 3D lattice for curved sandwich structures

Shuai Kang^{a,b}, Wenfeng Liu^{c,1}, Jiangtao Wang^{a,b}, Hongwei Song^{a,b,*}, Wu Yuan^{a,b},
Chenguang Huang^b

^a Key Laboratory for Mechanics in Fluid Solid Coupling Systems, Institute of Mechanics, Chinese Academy of Sciences, Beijing 100190, China

^b School of Engineering Science, University of Chinese Academy of Sciences, Beijing 100049, China

^c Institute of Physics, University of Amsterdam, Amsterdam 1098 XH, The Netherlands

ARTICLE INFO

Keywords:

Pinned
3D lattice
Curved sandwich structures
Self-adaption
Mechanical properties

ABSTRACT

The design and fabrication of curved sandwich structures with a 3D lattice core always faces the challenge of adaptability and connectivity between the core and the skins. Here, we propose a pinned method by releasing rotational degrees of freedom in the common node of the adjacent lattice cells. The design of the lattice core only needs to consider the size and number of cells rather than the shape of the skins. The pinned design demonstrates advantages in self-adaption of the 3D lattice core to skins with generalized cylindrical type and ensures to fabricate curved sandwich structures of a large scale. Lattice samples of four kinds of node-connection forms with three different strut thicknesses are fabricated to investigate the effects of pin-joint design and strut thickness on mechanical performance. Lattices with suitable collinear connection design have comparable modulus and strength to snap-fitted lattices. The proposed method has the potential for standardized production of curved 3D lattice sandwich structures with excellent mechanical performance.

1. Introduction

Reducing structure mass under the premise of ensuring mechanical properties and functional requirements is always an important subject. As important parts of load-bearing [1], lattice sandwich structures consist of two thin skins and a thick low-density core exhibit high specific stiffness [2–4], high specific strength [5–7], energy absorption [8–12], and multifunctional integration characteristics [13–15]. There is a major issue that restricts the lattice sandwich structures to be popped from laboratory to engineering sectors: the adaptability of the lattice core to curved skins to make a sandwich structure with complex shapes.

So far, the fabrication of lattice sandwich structures mainly focuses on the flat [16–23] and cylindrical structures. Large-sized carbon fiber reinforced sandwich shells with different types of cores are fabricated based on the filament winding and mold forming [24–28]. Tao et al. [29] propose a novel foam core sandwich-walled hollow column made of glass-reinforced polymer faces and polyvinyl chloride foam core. Xiong et al. [30] fabricate a kind of cylindrical metallic lattice cores by using wire cutting and interlocking methods through the overall design of longitudinal and transverse ribs. To completely adapt to assembled

pyramidal lattice cores, four additional auxiliary patch face sheets are made to eliminate assembly errors and prestress. Wang et al. [31] take advantage of the geometric mapping and snap-fitting method to fabricate the cylindrical full metallic sandwich with 3D pyramidal lattice cores. With the increasing complexity as well as the scale of engineering structures, the adaptability and reliability of the connection between the core and skins become more challenging. Traditional methods require complex customized design even sacrifice the local target shape to assemble. Deviation of the skin shape from the target shape will also affect its aerodynamic characteristics and load-bearing capacity [32, 33].

In recent years, the development of additive manufacturing technology makes it possible to achieve the rapid prototyping of multitudinous types of complex structures [9,34–36]. When employing a direct printing method to fabricate sandwich structures with a 3D lattice core, there leaves no adaptability problem, but the anisotropy from the printing direction may harm the mechanical performance [37–41]. Removal of support material and size of printing platform also limit the practical application of integral 3D printed lattice structures. Liu et al. [42,43] introduced the snap-fitting method into additive manufacturing

* Corresponding author at: Key Laboratory for Mechanics in Fluid Solid Coupling Systems, Institute of Mechanics, Chinese Academy of Sciences, Beijing 100190, China.

E-mail address: songhw@imech.ac.cn (H. Song).

¹ These authors contributed equally to this work and should be considered co-first authors.

technology, which achieves optimal mechanical properties of the struts. These works paved avenues for the fabrication of large-scale and sound performance 3D lattice sandwich panels with 3D printing. However, there are some limitations on the fabrication of lattice sandwich structures with curved surface skins by the snap-fitting method. The fabrication of curved sandwich structures by using the snap-fitting method requires pre-customized design and precise calculation. It is difficult for the snap-fitting method to give simple design criteria for curved sandwich structure with generalized cylindrical type skin and the reliability of the connection is questionable. The fabrication of a super-large sized lattice core is also easily restricted by the platform space of 3D printing. A more standardized and universal method that can achieve reliable connections between 3D lattice core and curved surface skins while maintaining optimal mechanical performance needs to be developed.

The discretization of cells into standard elements can reduce the structural complexity and makes the design much easier and more flexible to explore [7,44–46]. It is also inspiring that by using lattice representations of the rotating rigid mechanism, a class of 3D auxetic lattice structures that are capable of offering Poisson's ratio from positive to negative in a wide range is designed [10]. Based on the snap-fitting method [43] and the idea of rigid body discretization, we propose a novel fabrication method by releasing the rotational degrees of freedom in the common node of the adjacent cells and introducing pin-joints. The adaptability to curved surfaces and the possibility of fabricating large-sized lattice sandwich structures are discussed. Lattice samples of four kinds of common node forms with three different strut thicknesses are tested to investigate the effects of pin-joint design and strut size on mechanical performance. The suitable configuration of the pinned method to generalized cylinders is discussed. The proposed method can be extended to various material systems and other manufacturing techniques besides 3D printing, since the discretized standard element that makes pinned cells can be fabricated with various techniques, e.g., casting, cutting, etc.

2. Design of self-adaptive 3D lattice

2.1. Concept of pinned 3D lattice

For the traditional 3D lattice structure, the common node of adjacent cells can be regarded as a kind of fixed condition upon assembly, and cannot move or rotate with each other under the stress-free state. More degrees of freedom in the assembly process leads to more design space. The lattice cores can release the rotational degrees of freedom in the common node of adjacent cells by replacing the common node with the pin-joints to form pinned 3D lattice cores.

As shown in Fig. 1(a), a one-dimensional (1D) pinned cell group has a kind of pin-joint, which is deemed as an axis of rotation that is always perpendicular to the zy or xz plane, and the unit cell can be stacked only along the y -axis or x -axis. For every pinned cell group formed by two cells with a kind of pin-joint in lattice core, rotational state 1 and rotational state 2 only exist in one state at a time. During normal rotation between two adjacent physical interferences, the angle formed by the two rays of the strut axis at the initial position and the final position is the rotatable range. When the thickness of the struts and the volume of the node platforms are ignored, cell 2 is always regarded as an object of reference, and adjacent cell 1 can rotate either clockwise or counter-clockwise around the x -axis/ y -axis in the range close to 180° . The actual rotatable range is dependent on the specific design of pin-joints and is usually less than the ideal rotational range because of the physical interference constraint, which will be detailed in the next section.

As shown in Fig. 1(b), although the unit cell can be stacked in xy plane to form a larger two-dimensional cell group, adding the pin-joints that enable the lattice core to rotate in different directions does not generate a new number of rotational states around the axis. Rigid body rotation of the two cell groups keeps an orthogonality relation when rotating around different axes because of the physical interference constraint. For example, once rotation manipulation is carried out with cell group (1,4), it becomes infeasible to then carry out another rotation manipulation with cell group (3,4) since the pin joints have become misaligned.

As a result, the proposed concept can be applied to a generalized cylinder [47] in an existing form of connection because the pinned lattice core has the only direction of rotation and is independent of the type number of pin-joints. The length and crimp degree of the lattice array can be adjusted by the number of stacked cells and the rotation angle between adjacent cells.

2.2. Adaptability to curved surfaces

The rotatable feature of the pinned lattice core makes the node platforms contact flexibly to the skins of complex curved surfaces. The self-adaptive capability of the lattice core with mass production potential is illustrated in Fig. 2(a). The pinned lattice cell core with an unlimited number of rows and columns can be regarded as a kind of novel material system, which is named "lattice materials". It is just like a piece of cloth to be tailored and cut, and it can be rolled to form the preforms before shaping. Under customized load, the roll of lattice materials is self-adaptive to skins of complex curved surfaces, thereby completing the fabrication of the curved sandwich structures with 3D lattice core.

Three basic types of curved surfaces that the lattice core can adapt to

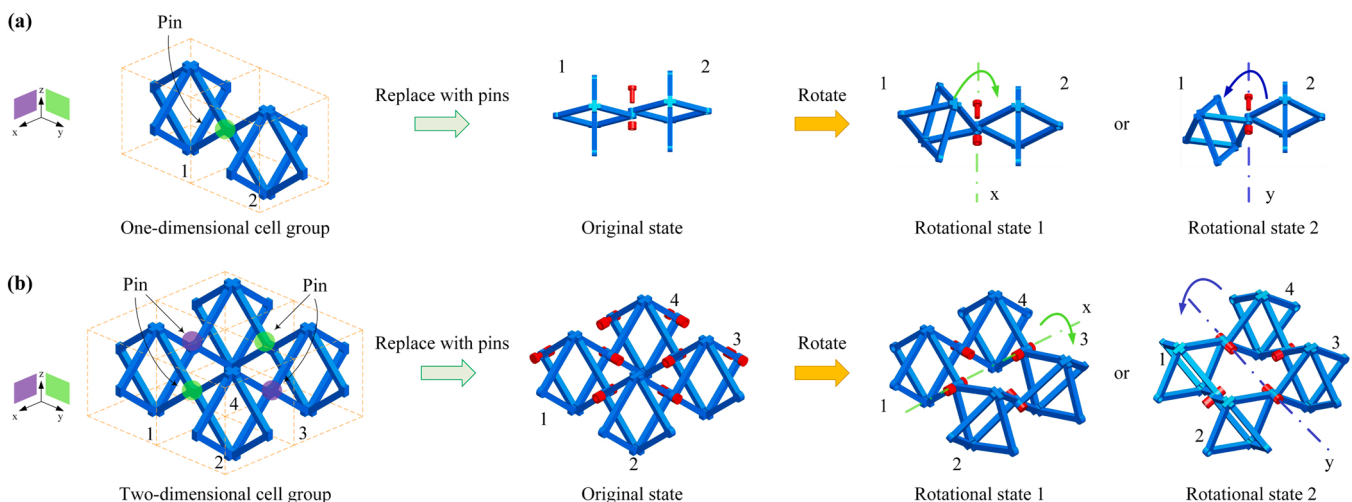


Fig. 1. Concept design of pinned lattice cores. The evolution process of (a) one-dimension (1D) cell group (b) two-dimensional (2D) cell group.

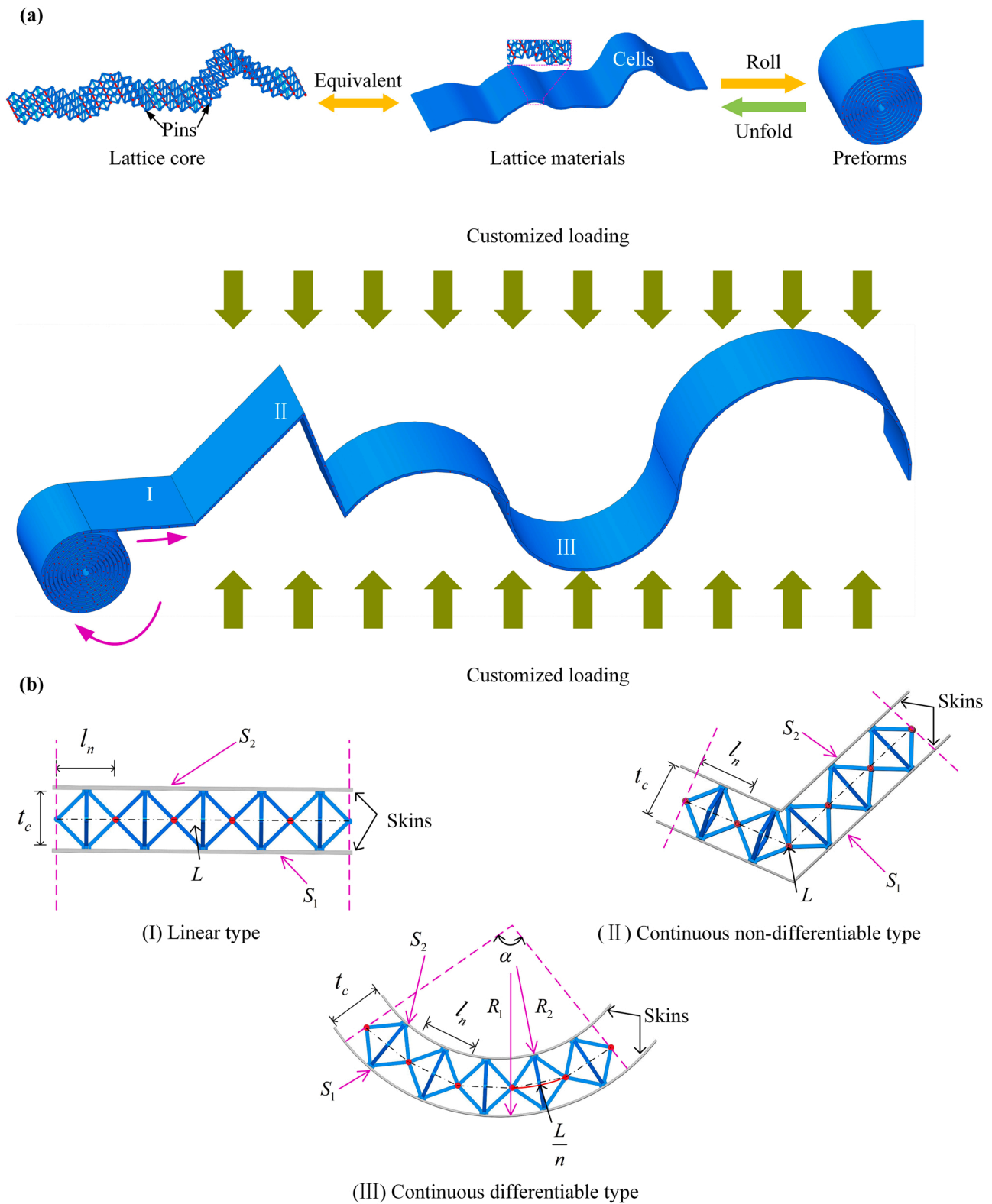


Fig. 2. Adaptability to curved surfaces. (a) the self-adaptive lattice core to complex curved surfaces with mass production potential; (b) three basic types of adaptable generalized cylinders.

sketched in Fig. 2(a) are detailed in Fig. 2(b). They are linear type (I), continuous non-differentiable type (II) and continuous differentiable type (III). The naming convention of three basic types arises from the characteristics of the function corresponding to the projection line of skins. These three basic types belong to the generalized cylinder [47],

which is defined as the trajectory generated by the moving line that moves along the fixed curve in space. The length of the central line (L) of different core shapes only depends on the distance of the adjacent pin-joints (l_n) and the number of cells (n). For the first two types of surfaces, $L = nl_n$. The length of the projection line of outside and inside

skins are defined as S_1 and S_2 , respectively. Relations between the length of the central line L and the length of the projection line of skins is expressed as

$$L = \frac{S_1 + S_2}{2} \tag{1}$$

The central line of the continuous differentiable type is an arc. The projection of pin-points is on the central line and the length of the curve between adjacent pin-points is $\frac{L}{n}$. The central angle corresponds to the sandwich structure with inner radius and outer radius R_1 and R_2 is defined as α . Relations between the geometry of the given cylinder type and the distance of the adjacent pin-joints (l_n) is expressed as:

$$n = \frac{\alpha}{\arcsin \frac{l_n}{R_1 + R_2}} \tag{2}$$

Where n is the number of the pinned cells.

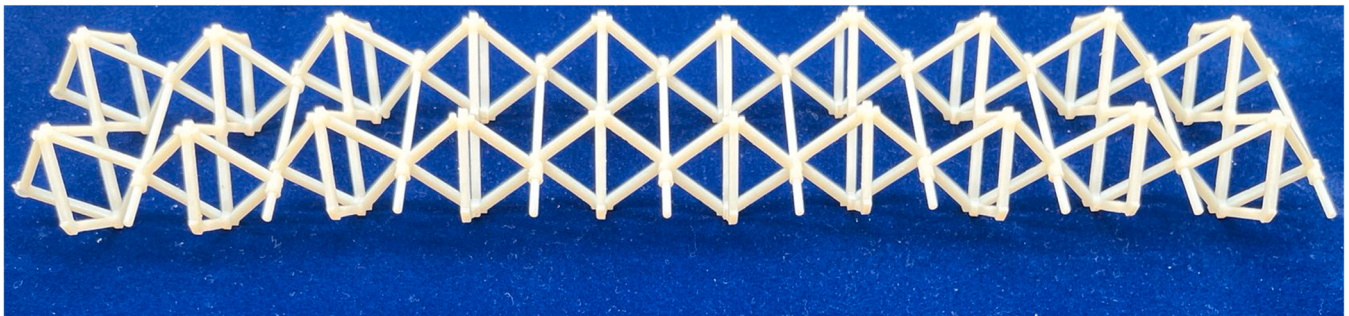
The length of the central line is obtained as follows:

$$L = \frac{R_1 + R_2}{2} \alpha = \frac{n(R_1 + R_2)}{2} \arcsin \frac{l_n}{R_1 + R_2} \tag{3}$$

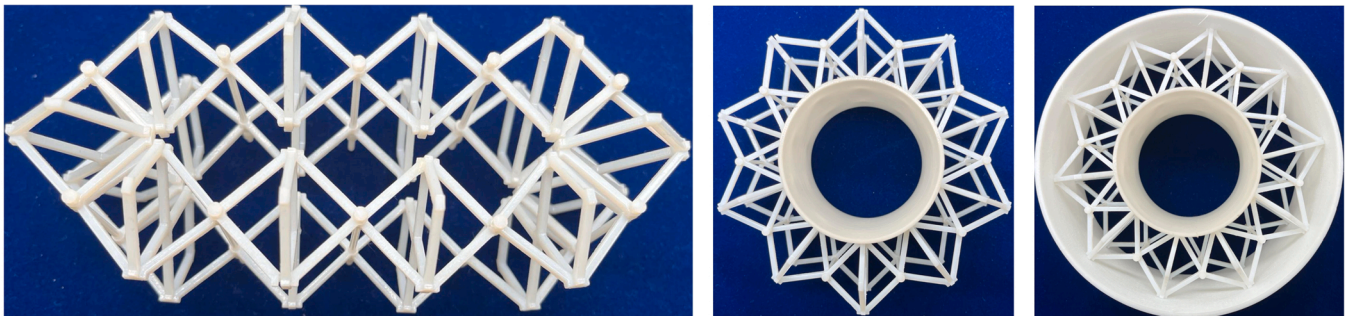
The pinned lattice cores can adapt to the arbitrarily generalized cylinders that are the combination of the three basic types by rotating the adjacent cells and designing the number and size of cells. Theoretically, the complexity of the geometry and the scale on the lattice sandwich can be arbitrarily adjusted by the number and size of cells.

2.3. Proof of adaptability

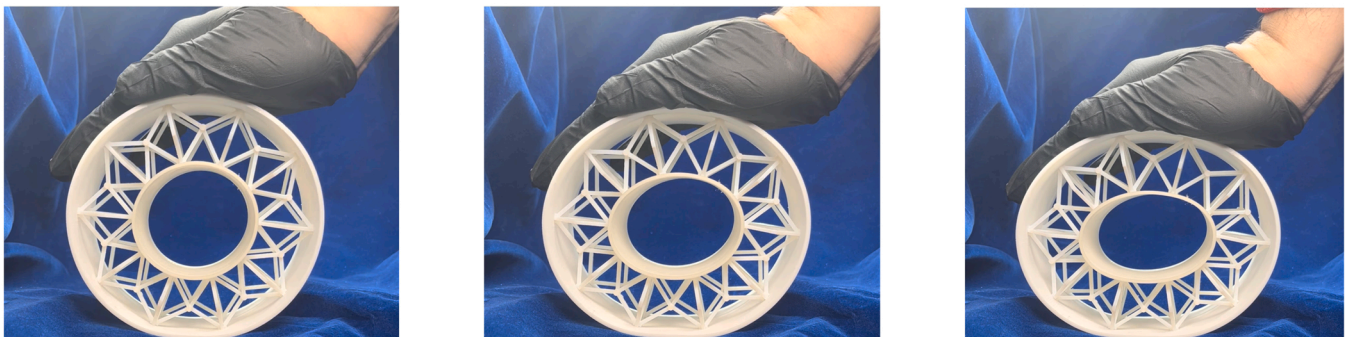
To verify the strong self-adaptation of the pinned lattice cores to the curved surface skins, we used the pinned method to manufacture lattice sandwich curved structures by additive manufacture (FDM and PloyJet). Fig. 3 shows the assembly process and the self-adaptive deformation of octahedral lattice sandwich structure under loading. Upon pressing, the pinned octahedral lattice core can be adjusted adaptively to the shape of the inner and outer skins and the nodes platforms contact to the skins do not separate from each other (also see the supplemented video). The



(a)



(b)



(c)

Fig. 3. Pinned lattice sandwich cylinder demonstrates self-adaptation (fabricated by TPU and RGD835). (a) unfolded pinned lattice core; (b) a complete lattice sandwich cylinder before curing; (c) the self-adaptive deformation under loading.

desired curved shape can be obtained and solidified after adhesive bonding in the common nodes and node's platform contact to skins.

Supplementary material related to this article can be found online at [doi:10.1016/j.addma.2022.102761](https://doi.org/10.1016/j.addma.2022.102761).

Fig. 4 demonstrates three large-sized pinned octahedral lattice sandwich shells fabricated by the present method. The skins were printed with PLA plus and the lattice core was printed with RGD835. The connection between lattice core and skins and pin-joints are bonded with superglue (cyanoacrylate). The maximum feature length for the wing-shaped shell is close to 300 mm and the heart-shaped shell is close to 150 mm. The pinned method is universal and is not limited by the size of the fabrication platform. The large-sized special-shaped sandwich shell needed in engineering applications can be realized by suitable parent materials. The proposed method can be extended to other additive manufacturing techniques besides 3D printing (FDM and PloyJet), since the discretized standard elements to make pinned cells can be fabricated with various techniques, e.g., casting, cutting, etc.

3. Fabrication and mechanical behaviors

3.1. Design of pin-joints

The connection forms of pin-joints may influence the mechanical performance of lattice samples, so it is essential to design suitable pin-joints. As shown in Table 1, three kinds of pin-joints that have only one kind of allowable rotation direction are exhibited to design different connection forms. According to the projection of the axis of the strut alignment, the pin-joints can be divided into the non-collinear type and collinear type. As shown in Fig. 5, the rotatable range of non-collinear type and collinear type is 6.8° – 173.2° and 66.3° – 113.6° , respectively. The collinear-1 type and the collinear-2 type have the same rotatable range because of some of the same design details. The strut thickness at pin-joint in the non-collinear type is the same as the thickness of struts whereas the collinear type is reduced by half. For the non-collinear type and collinear-1 type, the two rings on the two adjacent matching parts are fitted and the pins are then inserted into the two rings with the same axis to form a complete pin-joint. The most striking difference between the collinear-1 type and the collinear-2 type is that the latter needs no additional pins, and uses its convex and annular grooves as a part of the pin-joints. The thickness of the convex and the cushion cap in collinear-2

type is half of the thickness of the struts. The diameter of each pin (d) corresponding to a different connection type is consistent with the thickness of the struts. The outer diameter (D) of each ring of the pinned type is slightly larger than that in the snap-fit type to ensure that the cross-sections of the connecting areas are approximately equal. For the non-collinear type and the collinear-1 type, the length of the front end of the pin is equal to the sum of the thickness of the struts at the pin-joints and the thickness of the cap ($m = n + 2t$). For the collinear-2 type, the length of the front end of the pin is equal to the sum of the thickness of the struts at the pin-joints ($m = n + t$). The variational geometric parameters are shown in Table 2.

3.2. Fabrication of lattice samples

The octahedral lattice samples in Fig. 6 were fabricated by PloyJet technology and the snap-fitting method. All components of lattice samples were printed with VeroWhitePlus (RGD835) model and SUP706 support material on a Stratasys Objet30pro printer and had optimal build direction. Two-dimensional lattice parts, pin-joints, and planes were orthogonally snap-fitted into each other to form 3D lattice sandwich structures. To ensure a smooth snap-fit, the splicing notch retains a 0.06–0.08 mm printing margin. The nodes among the lattice cores, planes, and pinned joints are bonded with superglue (cyanoacrylate) to prevent the separation of parts during the entire fabrications and experiments.

The geometric parameters of assembly parts of four different connection types are shown in Fig. 6(a), (b), (c), and (d), respectively. In Fig. 6(a), the snap-fitted lattice proposed by Liu et al. [43] is taken as a comparison basis, whereas Fig. 6(b), (c), and (d) correspond to connection forms listed in Table 1. The cross-section of the struts of the lattice cores is square. The struts with a length $l = 18$ mm, are consistent in different lattice samples. The angle between the oblique beam and the horizontal line is 45° . The width of node platforms, a , is 4.6 mm. The other variational geometric parameters of models with different kinds of connection forms and strut thicknesses are shown in Table 2.

3.3. Experimental study and numerical simulation

To verify the effect of different connection forms on the mechanical behavior of lattice samples with different strut thicknesses, a series of

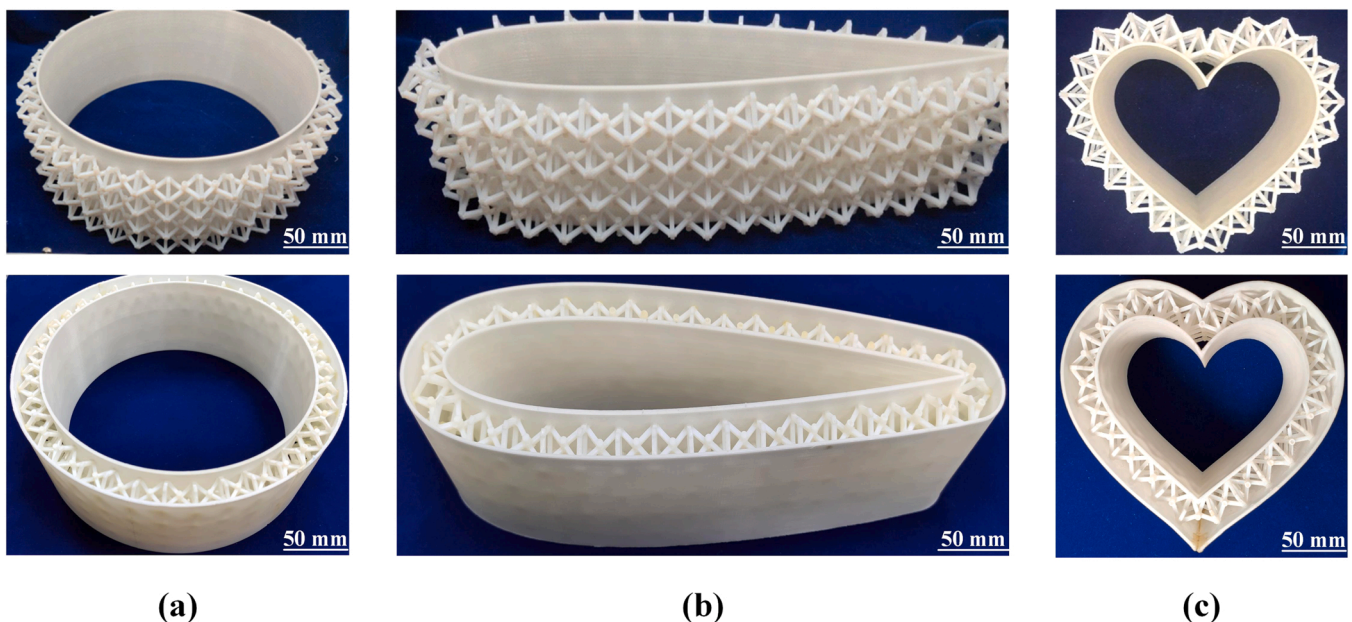
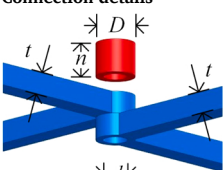
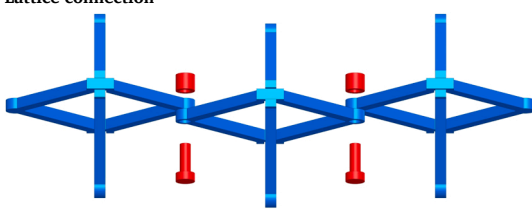
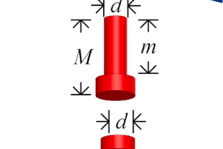
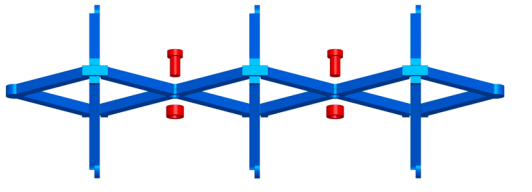
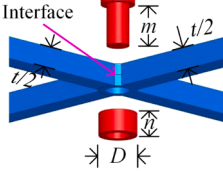
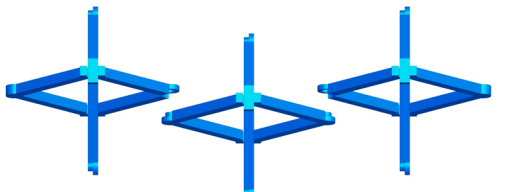


Fig. 4. Large-sized sandwich shells with octahedral lattice core. (a) cylindrical sandwich shell; (b) wing-shaped sandwich shell; (c) heart-shaped sandwich shell.

Table 1
Three kinds of pin-joints and design details.

| Connection type | Connection details | Lattice connection | Rotatable range |
|-----------------|---|--|-----------------|
| Non-collinear |  |  | 6.8° ~ 173.2° |
| Collinear-1 |  |  | 66.3° ~ 113.6° |
| Collinear-2 |  |  | 66.3° ~ 113.6° |

out-of-plane compression tests were conducted in a uniaxial testing machine (SUST CMT5205) at a nominal crosshead rate of 0.5 mm/min.

The compressive stress-strain curves and failure modes of specimens with different connection forms and strut thickness were shown in Figs. 7–9. In all cases, after the initial preload, the stress linearly increased with an increasing strain until an initial peak was reached. Continued loading resulted in rapid softening. With the loading process, the local large deformation or brittle fracture often occurred nearby pin-joints but the debonding of the pin-joints did not appear during the compression process. Compared with the other two designs types, the collinear types always suffered from the brittle fracture in the post-buckling stage, which resulted from the weakening of the thickness of the pin-joints. The maximum compressive strain was uniformly limited to 0.18.

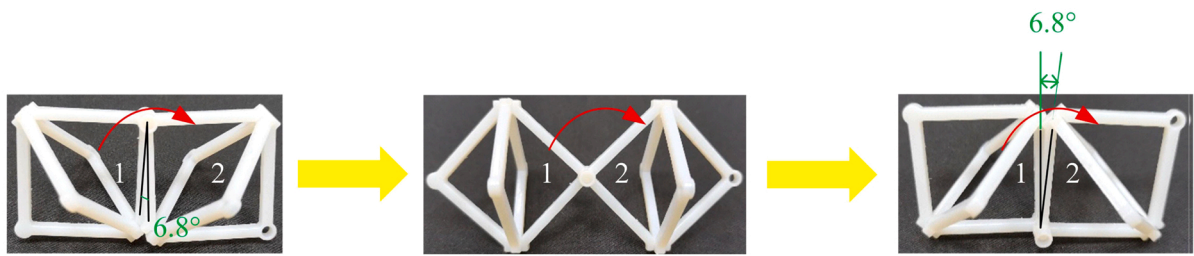
The stress-strain responses and failure modes of the lattice samples with different connection forms and 1.5 mm strut thickness were shown in Fig. 7. The snap-fit type and the non-collinear type reached their initial peak stress of 0.038 MPa and 0.043 MPa at a strain of 0.057 and 0.065, respectively. Then the stresses dropped rapidly due to the buckling of the struts and no obvious fracture occurred in the post-buckling stage. In contrast, the collinear-1 type had the highest peak value of 0.048 MPa at the strain of 0.06 among the four assembly forms and showed an obvious continuous fracture and even catastrophic failure after the peak because of the weakening of struts near the pin-joints. The stress concentration caused by insufficient cementing and solidifying made the struts more likely to fracture nearby the pin-joints. The collinear-2 type reached its initial peak strength of 0.042 MPa at a strain of 0.050. The trend in the post-buckling stage was gradually consistent with the snap-fit type. It is found that the stress of the snap-fit type was always the lowest among the four tested types before the peak stress was reached. This phenomenon was repeatable after the experiments several times. The reason for such a result is that stress concentration appears at the nodes of the snap-fit type, whereas the connection nodes of a pinned type are strengthened by solidified superglue.

Fig. 8 showed compressive responses and failure modes of the lattice samples with four connection forms and 2.0 mm strut thickness. The

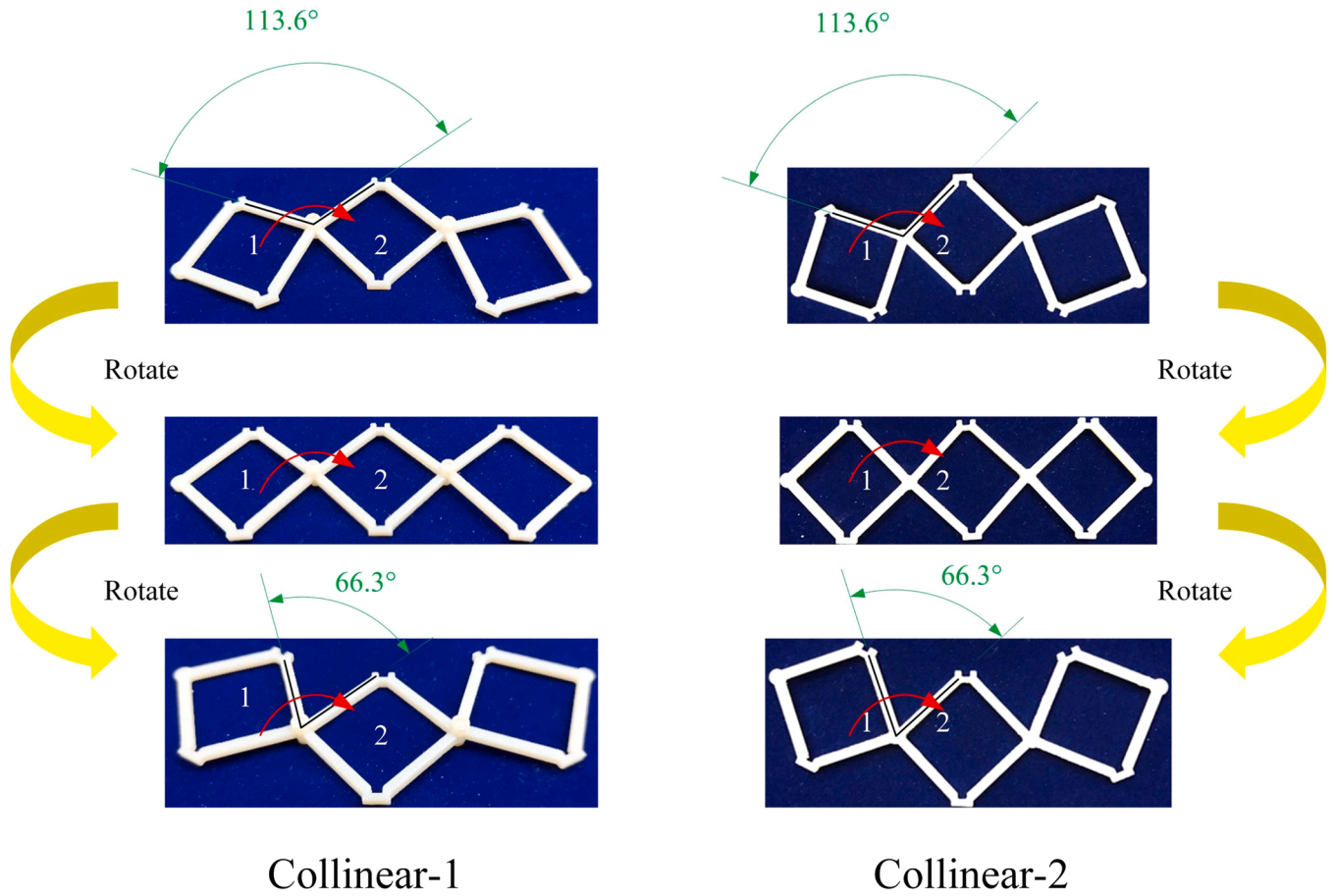
snap-fit type and the non-collinear type reached their initial peak stress of 0.108 MPa and 0.093 MPa at a strain of 0.06 and 0.086, respectively. Then the stresses dropped rapidly due to the buckling of the struts and no obvious fracture occurred in the post-buckling stage. The collinear-1 type had the highest peak value of 0.114 MPa at the strain of 0.054 among the four types. The post-buckling stage was characterized by continuous fracture but no catastrophic failure due to the increase in strut thickness. In contrast, the collinear-2 type had a lower peak value and strut breakage with the increase of load. This explanation is verified by the numerical results that will be given in the latter part of this section.

Compressive responses and failure modes of the lattice samples with strut thickness 2.5 mm are shown in Fig. 9. The snap-fit type and the non-collinear type reached their initial peak stress of 0.28 MPa and 0.229 MPa at a strain of 0.063 and 0.083, respectively. Then the stresses dropped rapidly due to the buckling of the struts and no obvious fracture occurred in the post-buckling stage. The collinear-1 type had the highest peak value of 0.304 MPa at the strain of 0.070 among the four types. The collinear-2 type reached its initial peak strength value of 0.246 MPa at a strain of 0.058. It is worth noting that continuous fracture occurs for the two collinear types compared to $t = 2.0$ mm, which is caused by the detailed design difference of the pin-joints between $t = 2.0$ mm and $t = 2.5$ mm.

The deformation behaviors of lattice samples are also investigated using finite element method (FEM) analysis, as shown in Fig. 10. The models of the lattice samples with octahedral core are based on the geometry of the test specimens in Table 2. The elastic-plastic material constitutive model was adopted for the finite element analysis. The elastic modulus and yield strengths are 1400 MPa and 69.2 MPa, respectively. The dynamic explicit step has been used to gain insight into the deformation behaviors of the whole lattice sandwich and the local area near the connection. All loading end nodes at the top surface are coupled with a central reference point with a linked rigid body. The simulations are subjected to displacement-control, using large displacement theory. The clamped boundary condition is set at the bottom surface of the lattice plane. In the three-dimensional finite



Non-collinear



Collinear-1

Collinear-2

Fig. 5. The actual rotatable range of different connection forms.

Table 2
Design parameters for the lattice samples with different connection forms and strut thicknesses (unit: mm).

| t | Connection Type | d | D | e | m | M | n | R | r | w | $\bar{\rho}$ |
|-----|-----------------|------|------|------|-----|-----|-----|------|------|------|--------------|
| 1.5 | Snap-fit | 3.09 | / | 2.33 | / | / | / | / | / | 1.62 | 1.36% |
| | Non-collinear | 1.5 | 3.26 | / | 4.5 | 6 | 2.5 | 1.63 | 0.83 | | 1.62% |
| | Collinear-1 | 1.5 | 3.26 | / | 3 | 4.5 | 2.5 | 1.63 | 0.83 | | 1.56% |
| 2.0 | Collinear-2 | 1.5 | 3.26 | / | / | / | / | / | / | 2.12 | 1.43% |
| | Snap-fit | 3.45 | / | 2.4 | / | / | / | / | / | | 2.29% |
| | Non-collinear | 2 | 3.5 | / | 6 | 8 | 3 | 1.75 | 1.08 | | 2.55% |
| 2.5 | Collinear-1 | 2 | 3.5 | / | 4 | 6 | 3 | 1.75 | 1.08 | 2.67 | 2.35% |
| | Collinear-2 | 2 | 3.5 | / | / | / | / | / | / | | 2.31% |
| | Snap-fit | 4.25 | / | 2.45 | / | / | / | / | / | | 3.44% |
| 2.5 | Non-collinear | 2.5 | 4.32 | / | 7.5 | 10 | 3.5 | 2.15 | 1.33 | 2.67 | 3.77% |
| | Collinear-1 | 2.5 | 4.32 | / | 5 | 7.5 | 3.5 | 2.15 | 1.33 | | 3.60% |
| | Collinear-2 | 2.5 | 4.32 | / | / | / | / | / | / | | 3.32% |

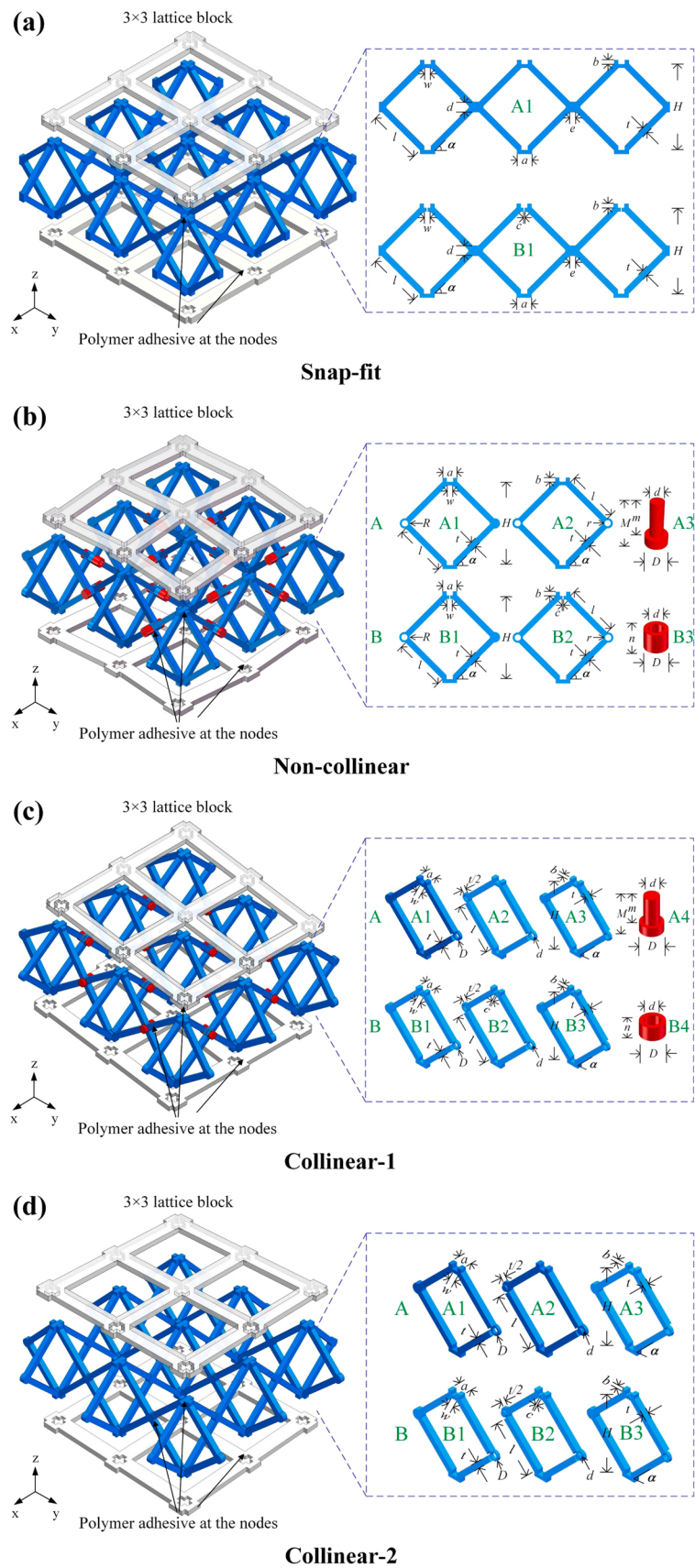


Fig. 6. The schematic diagram of lattice samples with different connection forms. (a) Snap-fit [43]; (b) Non-collinear; (c) Collinear-1; (d) Collinear-2.

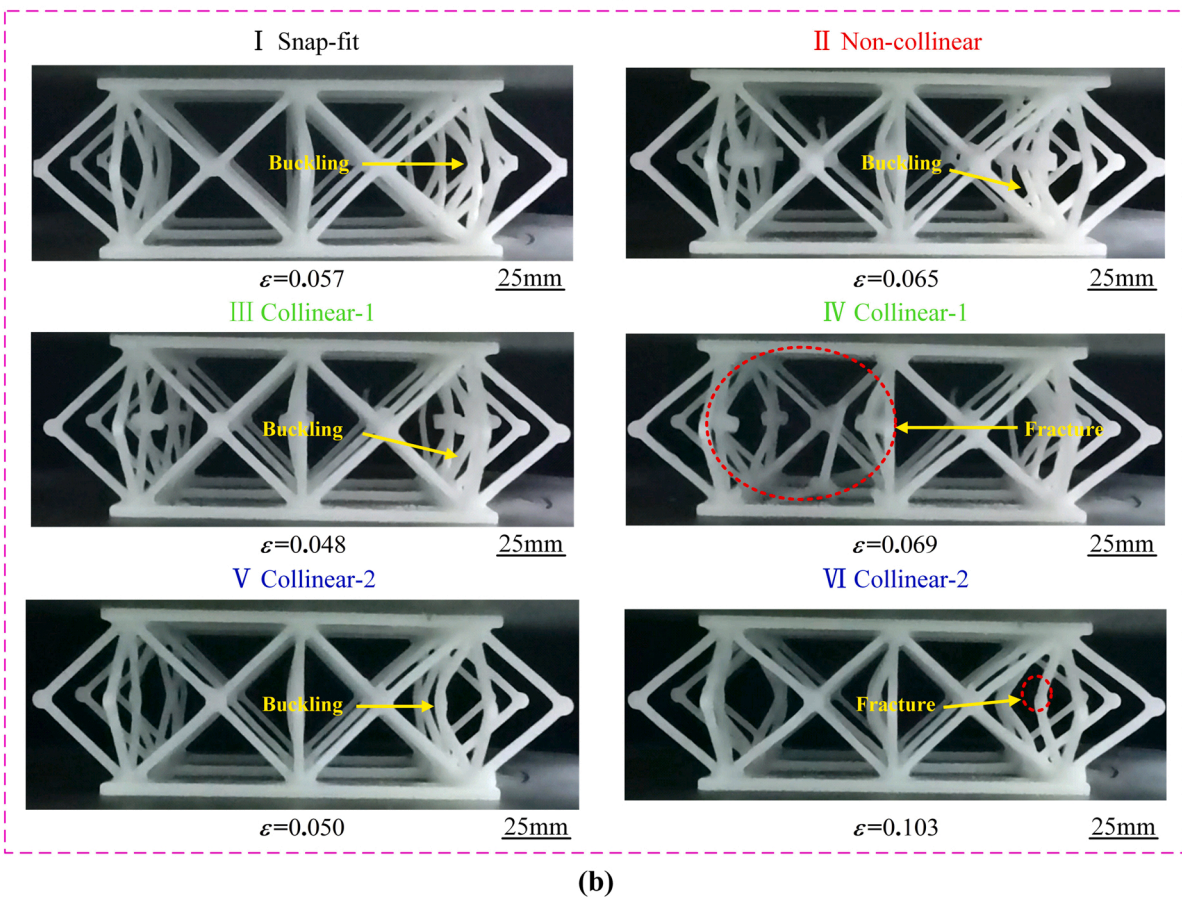
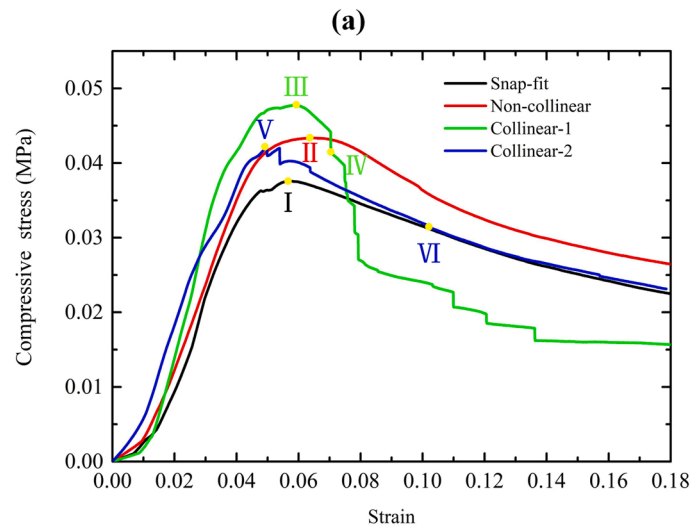
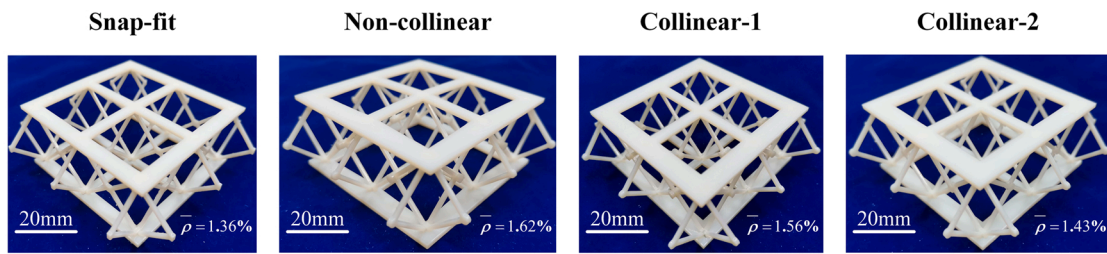
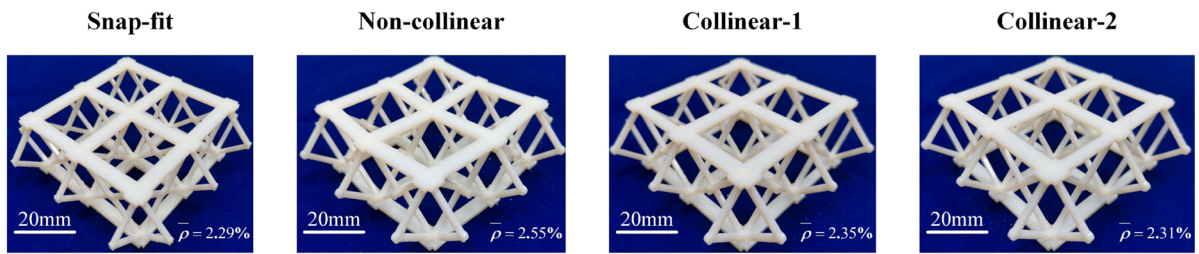
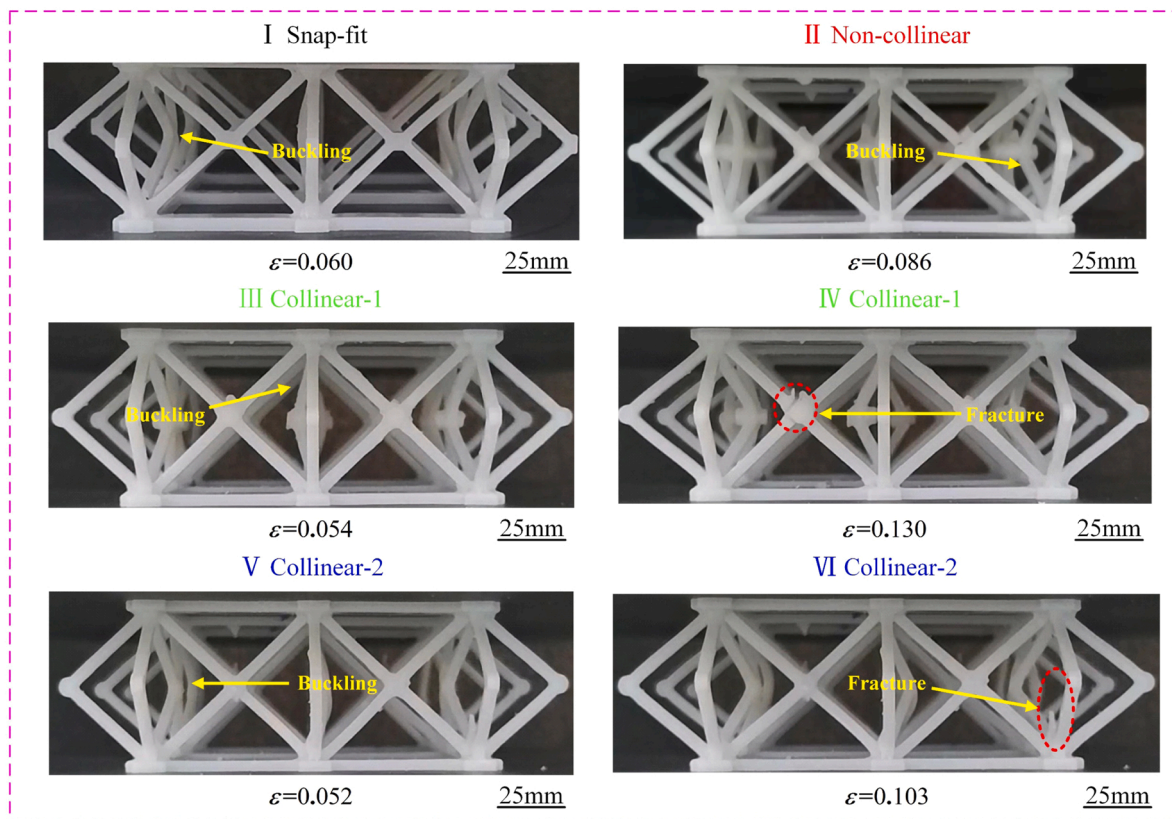
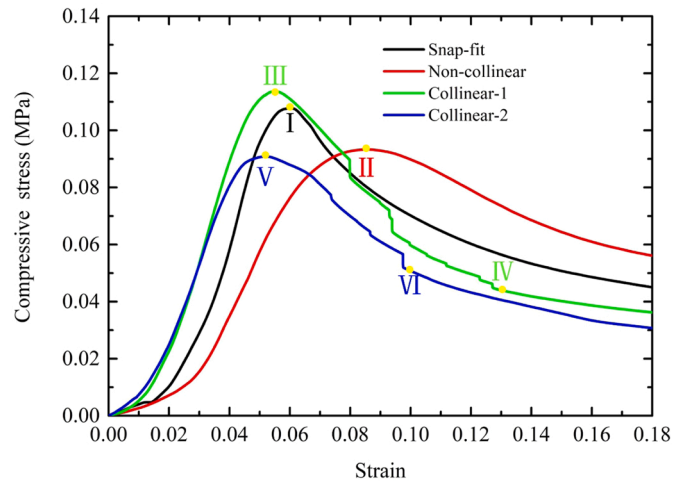


Fig. 7. (a) lattice samples and relative density $\bar{\rho}$. (b) stress-strain responses of octahedral lattice samples with different connection forms and failure modes. ($t = 1.5$ mm).

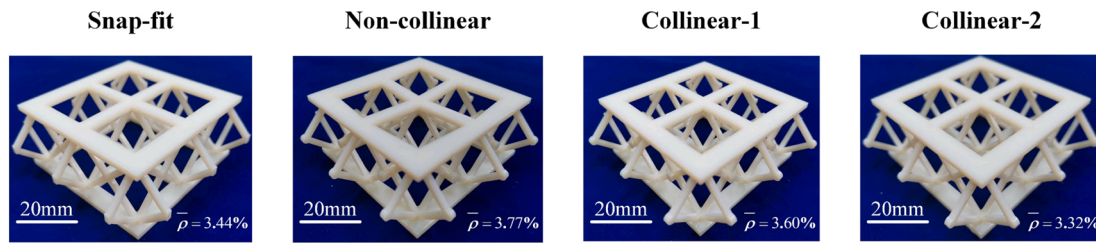


(a)

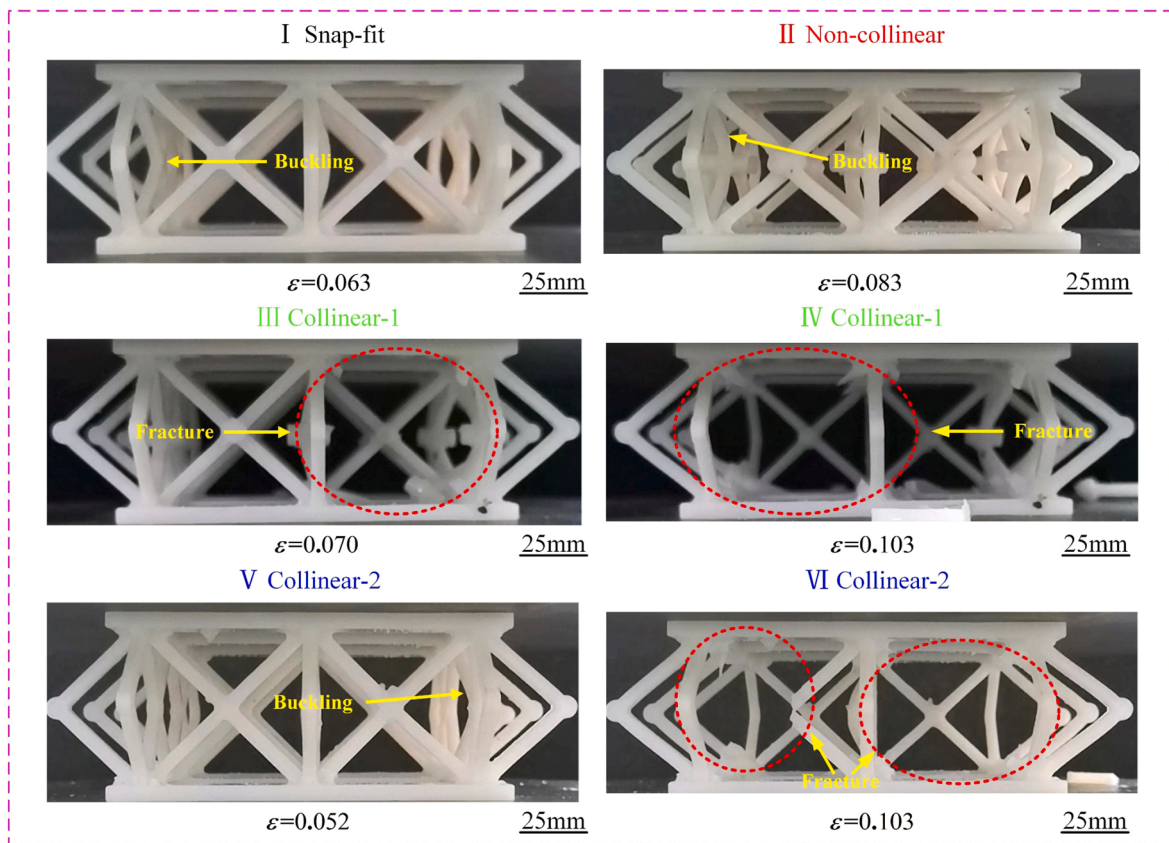
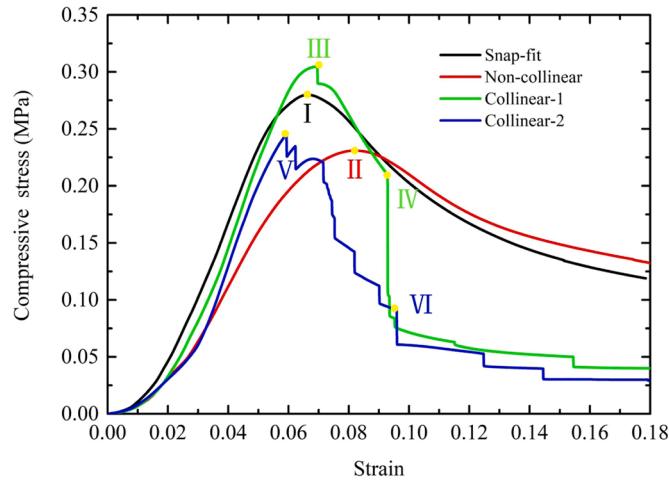


(b)

Fig. 8. (a) lattice samples and relative density $\bar{\rho}$. (b) stress-strain responses of octahedral lattice samples with different connection forms and failure modes. ($t = 2.0$ mm).



(a)



(b)

Fig. 9. (a) lattice samples and relative density $\bar{\rho}$. (b) stress-strain responses of octahedral lattice samples with different connection forms and failure modes. ($t = 2.5$ mm).

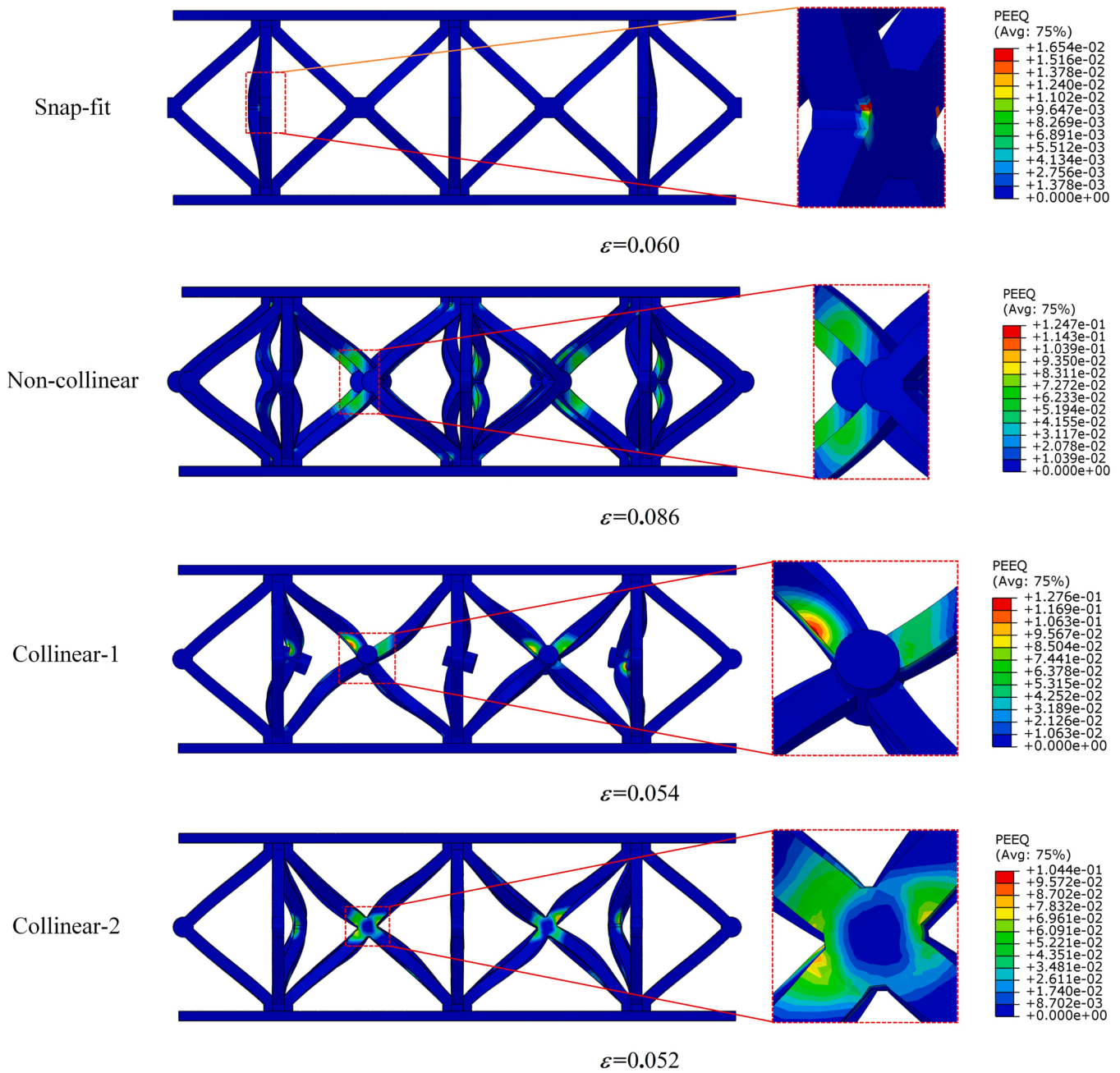


Fig. 10. FEM results of different connection forms with PEEQ at extreme point.

element models, 8-node linear brick 3D-stress reduced integration (C3D8R) elements are used. The models with the same connection forms and different thicknesses have similar deformation behaviors, so FEM results of different connection forms with a strut thickness of 2 mm are shown. For the snap-fit type, the largest equivalent plastic strain appears at the nodes. For the pinned types, however, when the load reaches the peak, the largest equivalent plastic strain always appears in the positions of struts near the connection nodes which has been strengthened. The numerical results are consistent with the experimental study since obvious large deformation and subsequent fracture are always observed in these positions.

The snap-fitting method has been considered to achieve the optimal mechanical properties of 3D-printed struts in previous studies [42,43], so we take it as the benchmark for further quantitative comparison. Collinear-1 type always has better performance in stress-strain curves. Comparisons of compressive modulus and compressive modulus

strength between two types with three different strut scales were shown in Fig. 11. Compared with the snap-fit type, compressive modulus of the collinear-1 type of the 1.5 mm, 2.0 mm, and 2.5 mm was increased by 38.82%, 45.01%, and 12.7%, respectively, and the compressive strengths of the collinear-1 type of the 1.5 mm, 2.0 mm, and 2.5 mm are increased by 26.32%, 21.99%, and 14.13%, respectively. With the increase of struts thickness, the advantage of the collinear-1 type over snap-fit type decreased gradually. At low density, it was obvious that the constraint and interaction of pin-joints improve the compressive performance of the lattice samples.

Considering that different connection forms will introduce a small difference in the relative density of lattice samples with the same strut thickness, a comparison of mechanical properties at the same relative density is necessary. According to the Gibson-Ashby equations [48], the relative modulus and relative strength have a power-law relationship with the relative density. Comparisons of relative modulus and relative

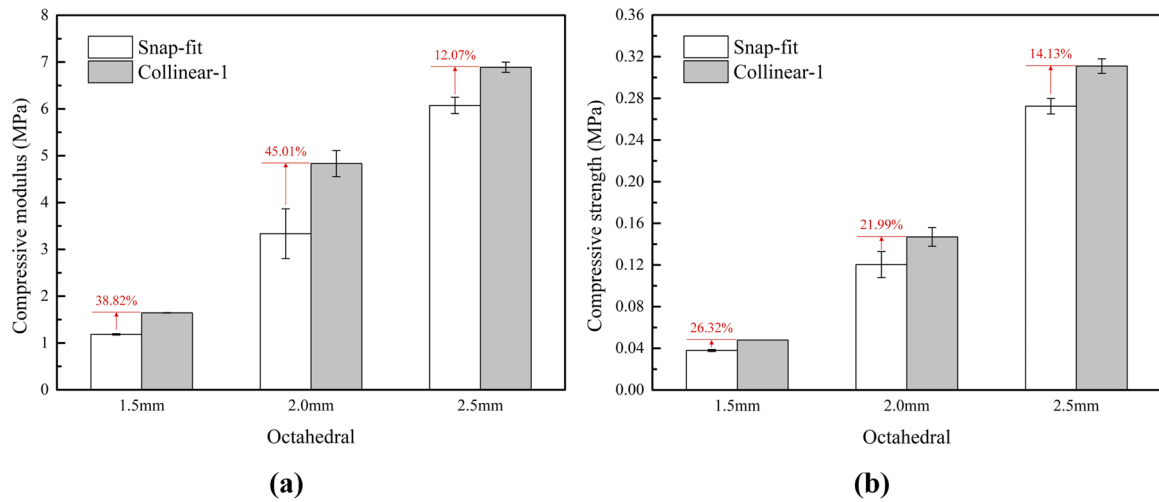


Fig. 11. Comparisons of mechanical performance of snap-fit type and collinear-1 type with different struts thickness: (a) compressive modulus and (b) compressive strength.

strength of lattice samples with different struts thickness fabricated by four kinds of connection forms were shown in Fig. 12. The fitted power-law parameter is shown in Table 3. Compressive modulus, E_{zz} , and compressive strength, σ_z^{pk} , are extracted from the corresponding stress-strain curves. E_s and σ_y are the elastic modulus and yield strengths of solid material, respectively. Judging from the results of the three kinds of struts thickness, the mechanical properties in the same relative density were evaluated from the connection forms, which were collinear-1 type, snap-fit type, collinear-2 type, non-collinear type in descending order. Significantly, although the pin-joints adds extra mass, the collinear-1 type was always better than the snap-fit type in the same relative density because the strengthened pin-points inhibit the rotation of the struts ends and resist out-of-plane bending deformation. In theory, the collinear-2 type should have the same performance as the snap-fit type, however, the adhesion of two half-thickness struts at the pin-joints of the collinear-2 type weakened the mechanical performance. The misalignment of the axis in the design of the non-collinear type will generate extra bending moment at the pin-joints, leading to early failure of the lattice struts under the combined action of bending and compression. With the increase of strut thickness, the bending moment at the common nodes increases, which is the reason why the red curve representing the mechanical properties of the non-collinear type in the figure deviates more and more from other curves.

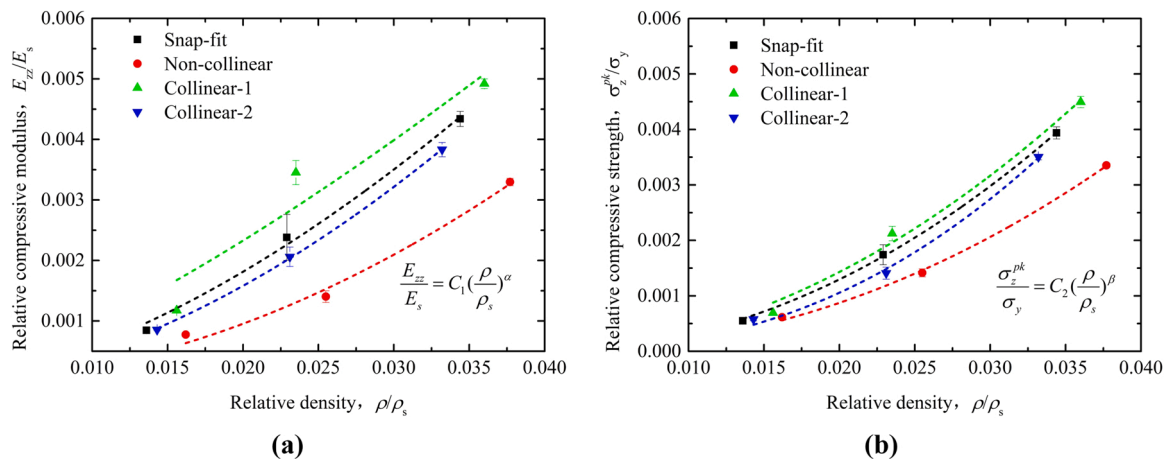


Fig. 12. Comparisons of mechanical performance of lattice samples with four connection forms: (a) relative compressive modulus and (b) relative compressive strength. (For interpretation of the references to colour in this figure, the reader is referred to the web version of this article.)

Table 3

The best fitting result of power-law for the mechanical properties of octahedral lattice.

| Connection Type | Relative compressive modulus | | | Relative compressive strength | | |
|-----------------|------------------------------|----------|-------|-------------------------------|---------|-------|
| | C_1 | α | R^2 | C_2 | β | R^2 |
| Snap-fit | 1.037 | 1.623 | 0.990 | 3.976 | 2.052 | 0.999 |
| Non-collinear | 1.885 | 1.939 | 0.979 | 3.438 | 2.116 | 0.997 |
| Collinear-1 | 0.418 | 1.327 | 0.832 | 3.068 | 1.961 | 0.983 |
| Collinear-2 | 1.489 | 1.75 | 0.999 | 10.653 | 2.356 | 0.991 |

3.4. Comparison of theoretical models with experiments

3.4.1. Theoretical models of snap-fitted octahedral lattice samples

The detailed design of the pin-joints and the non-coplanar axis of the struts make the stress state of the octahedral lattice samples very complicated. So, we set up a theoretical model based on the configuration of the snap-fit type. The octahedral structure can be referred to the derivation of body-centered cubic [42]. The final formula has been provided in this part.

The peak strength, σ_{pk} , of the octahedral unit cell is given by [18].

$$\sigma_{pk} = \frac{4F_z}{A_{cell}^{Oct}} = 2\sqrt{2} \frac{t^2}{A_{cell}^{Oct} \sigma_N} \quad (4)$$

Where $A_{cell}^{Oct} = (\sqrt{2}l + t + a)^2$ is the cross-sectional area of the octahedral unit cell, referring to Fig. 5(a). σ_N is the axial stress of the struts. The most common failure modes of lattice cores are yield, elastic buckling and inelastic buckling. The strength σ_N is obtained by σ_y , σ_E and σ_{IE} , respectively. The elastic buckling stress and inelastic buckling stress of struts in octahedral unit cell are given by [49].

$$\sigma_E = \frac{k^2 \pi^2 E_s}{12} \left(\frac{t}{l}\right)^2 \quad (5)$$

$$\sigma_{IE} = \frac{k^2 \pi^2 E_t}{12} \left(\frac{t}{l}\right)^2 \quad (6)$$

Where the k is determined by the end conditions on the buckling struts: for octahedral lattice unit cell in the actual compression process, one end of the strut is pin-jointed and the other is a built-condition, so $k^2 \approx 2$. E_t is the tangent modulus of solid material.

The effective modulus E_{zz} of the octahedral lattice is given by

$$E_{zz} = \frac{\sigma_z^{pk}}{\varepsilon_z} = \frac{2t^2}{3} \frac{H}{lA} E_s \quad (7)$$

Where the ε_z is defined as the strain of lattice structure along z direction.

3.4.2. Comparisons with predictions

The small solid cylindrical samples with a bottom diameter of 12.5 mm and a height of 25 mm from two different batches (RGD835) printed in X direction were tested in compression at speed 0.5 mm/min. The measured elastic modulus and yield strengths are 1400 MPa and 69.2 MPa, respectively.

Comparisons of relative compressive modulus and relative compressive strength between predictions and measurements in the different connection forms are shown in Fig. 13. It can be observed that the theoretical value is higher than the experimental value in Fig. 13(a). The sliding and deformation of the struts in the analysis model are only in the two-dimensional plane, and the further deterioration of stiffness caused by out-of-plane deformation is not considered in the actual compression process. The initial defects often make lattice structures bear the bending effect earlier and reduce their resistance to elastic deformation as well [42]. The effect of defects on compressive modulus increases with the decrease of size, which is consistent with the experimental results. As shown in Fig. 13(b), the peak strengths of the three struts scale for the four kinds of connection forms are captured by the inelastic buckling models. The theoretically predicted values are in good agreement with the experimental values for the snap-fit type and the collinear-2 type. The reason why the experimental value of the

collinear-1 type is higher than the theoretical value is that the extra mass of pin-points inhibits the rotation of the struts ends and increases the strength of the struts. The misalignment of the axis in the design of the non-collinear type will generate extra bending moment at the pin-joints, leading to buckling failure more easily.

4. Discussion

The pinned method originates from the discretization design idea. Similarly, the pinned octahedral lattice sandwich can be extended to general configuration by structural discretization. The $2 \times 2 \times 1$ lattice core is discretized and two directions of rotation axis are introduced, as shown in Fig. 14(a). By utilizing the symmetry of the lattice core, the case of cell arrays rotating around different axes can be simplified to two adjacent cells rotating around a single axis. The effect of the number of pin-joints and layer of pinned snap-fitting lattice cores are discussed in Fig. 14(b). If there is more than one common node between the two adjacent cells, the system will become geometrically stable. Therefore, only one common node between two adjacent cells of the suitable configuration can be replaced by a kind of pin-joint. As the number of layers increases, each cell will have redundant constraints due to the pin-joints in different planes, and the lattice core will form a rigid body. Therefore, the selection criteria of lattice configuration for intercellular characteristics can be summarized as follows:

- (1) There is only one common node between adjacent cells of the configuration;
- (2) The lattice core can only be a single layer.

The pinned method is derived from the snap-fitting method, so the intercellular characteristics of the two methods are consistent. The complete pinned unit cell also consists of two orthogonal inserts. As shown in Fig. 15(a), we use the projection of the nodes to illustrate. The brown dots represent the projections of the four outermost nodes of the configuration. The characteristic parallelogram is the projection of the unit cell in the xy plane. The position of the interlocking node (the blue dot) is within the closed area formed by the projections of the pin-joints (a quadrilateral formed by red lines). The diagonals of the quadrilateral are parallel to the two basic vector directions (orientations of the cells array), respectively. The projections of the internal nodes of the cell cannot exceed the boundary of the quadrilateral and should not coincide with the projection of the interlocking node.

Considering the intercellular and internal characteristics, the pyramid configuration is also suitable for the pinned method. As shown in Fig. 15(b), the pyramid configuration releases the rotational degrees of

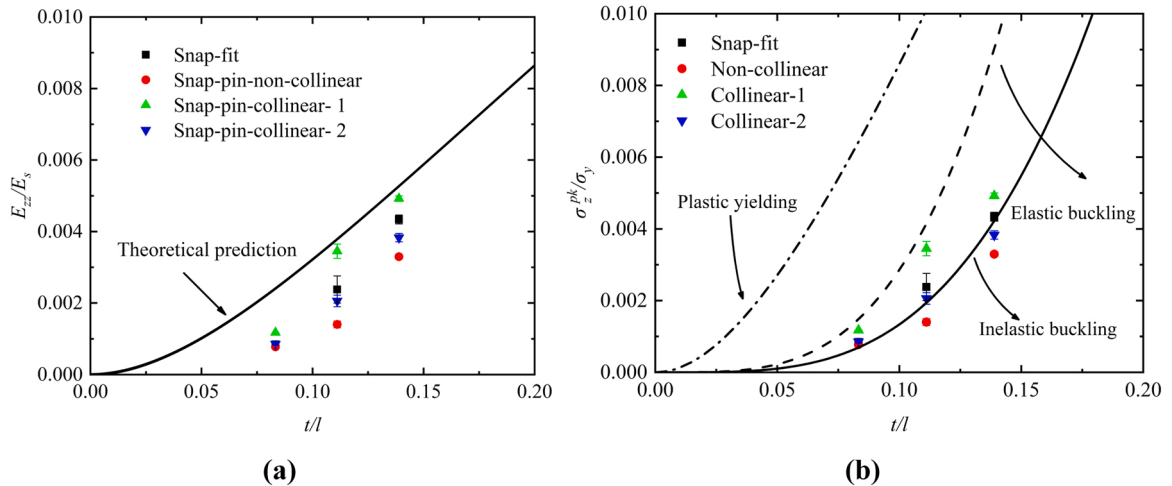


Fig. 13. Comparisons of (a) relative compressive modulus and (b) relative compressive strength of octahedral configuration between predictions and measurements.

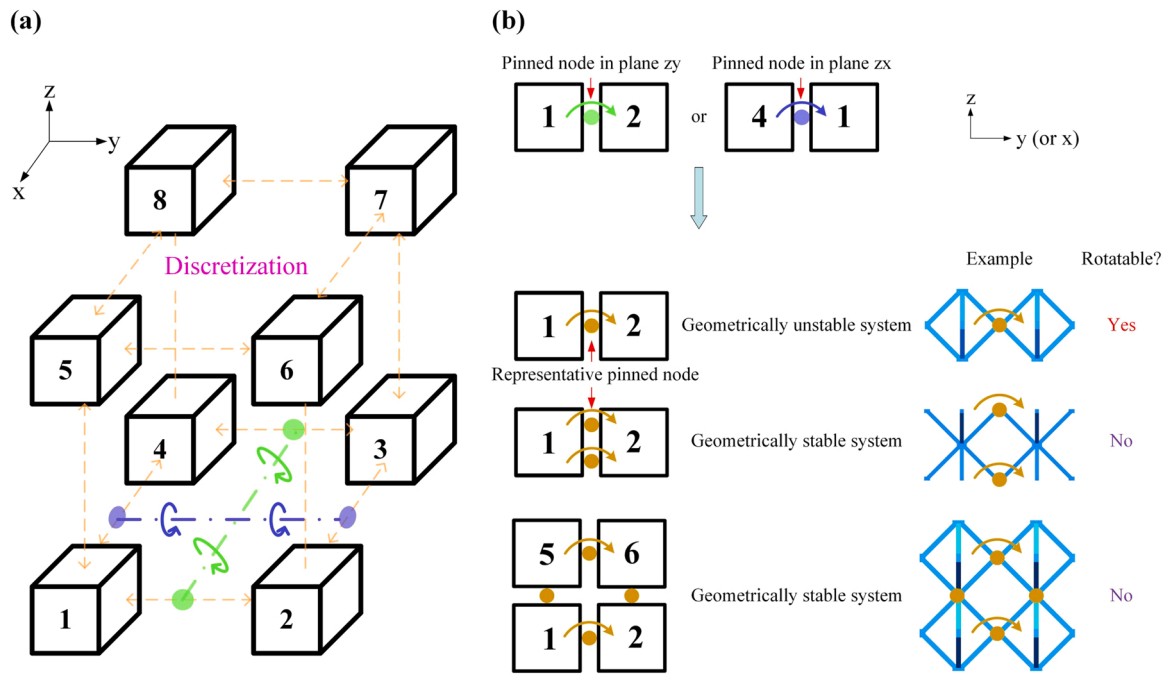


Fig. 14. The selection criteria for intercellular characteristics. (a) the discretization of general lattice cores; (b) effect of the number of core layers and pin-joints between two adjacent cells.

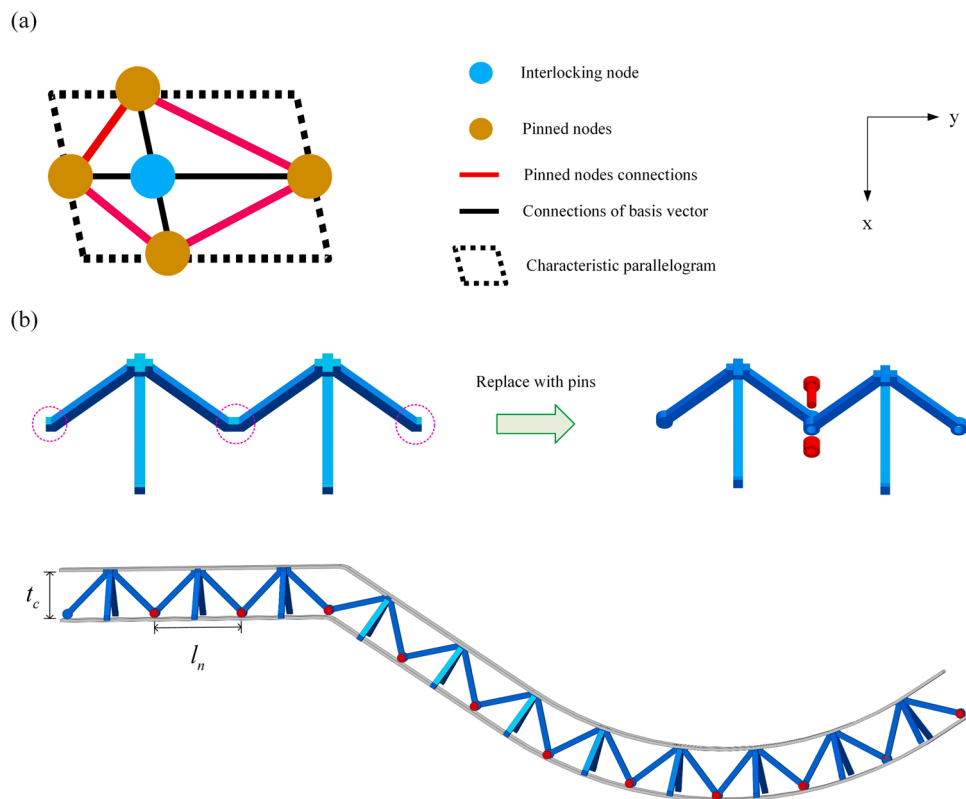


Fig. 15. The selection criteria for internal characteristics of the unit cell. (a) the projection characteristics of suitable configurations; (b) the pyramid configuration satisfying pinned method and curved surface skins.(For interpretation of the references to colour in this figure, the reader is referred to the web version of this article.)

freedom in the common node of adjacent cells by replacing the common node with the pin-joints to form pinned 3D lattice cores. The pinned pyramid lattice core can adapt to the curved surfaces by rotating the adjacent cells. Since the pinned nodes are also nodes that connect with

skins, the curvature adaptability of a pyramidal lattice is weaker than that of octahedral.

5. Conclusion

A pinned 3D lattice is proposed for the fabrication of curved sandwich structures. By releasing rotational degrees of freedom in the common nodes of the adjacent cells, a broad design space can be explored. The pinned lattice core can be adjusted adaptively with the inner and outer skins to form a curved lattice sandwich with a generalized cylindrical type. Large-sized octahedral lattice sandwich structures with curved surface skins are also designed and fabricated to verify adaptability. This method finds an easier standardized production for the fabrication of large-sized 3D lattice sandwich structures with curved surface skins in engineering applications by different fabrication technology and suitable materials.

Octahedral lattice samples in four kinds of connection forms with three different strut thicknesses are fabricated to investigate the effect of scale and pin-joint forms on mechanical performance. It is found that the lattice samples with collinear-1 type connection form have the highest compressive modulus and strength. Compared with the snap-fit type, compressive modulus of the collinear-1 type of the 1.5 mm, 2.0 mm, and 2.5 mm are increased by 38.82%, 45.01%, and 12.7%, respectively, and the compressive strengths of the collinear-1 type of the 1.5 mm, 2.0 mm, and 2.5 mm are increased by 26.32%, 21.99%, and 14.13%, respectively. The enhancement in the pin-joint nodes increases the compressive performance of the lattice block whereas also introduces brittle fracture.

The selection criteria of pinned lattice configurations have been discussed. More suitable lattice configurations and curved surface skins can be combined to form several special-shaped sandwich shell structures.

CRedit authorship contribution statement

Shuai Kang: Writing – review & editing, Writing – original draft, Methodology, Investigation, Data curation, Conceptualization. **Wenfeng Liu:** Writing – review & editing, Methodology, Investigation, Conceptualization. **Jiangtao Wang:** Writing – review & editing, Methodology, Investigation. **Hongwei Song:** Writing – review & editing, Supervision, Project administration, Methodology, Investigation, Conceptualization. **Wu Yuan:** Writing – review & editing, Supervision, Project administration. **Chenguang Huang:** Writing – review & editing, Supervision, Funding acquisition.

Declaration of Competing Interest

The authors declare that they have no known competing financial interests or personal relationships that could have appeared to influence the work reported in this paper.

Acknowledgement

Financial supports from the National Natural Science Foundation of China (Grant Nos., 11972035, 11902322, and 11972033), and Strategic Priority Research Program of the Chinese Academy of Sciences (Grant No. XDA22000000), are gratefully acknowledged.

References

- [1] M.F. Ashby, Y.J.M. Bréchet, Designing hybrid materials, *Acta Mater.* 51 (19) (2003) 5801–5821.
- [2] D.S.J. Al-Saedi, S.H. Masood, M. Faizan-Ur-Rab, A. Alomarah, P. Ponnusamy, Mechanical properties and energy absorption capability of functionally graded F2BCC lattice fabricated by SLM, *Mater. Des.* 144 (2018) 32–44.
- [3] T.A. Schaedler, A.J. Jacobsen, A. Torrents, A.E. Sorensen, J. Lian, J.R. Greer, L. Valdevit, W.B. Carter, Ultralight metallic microlattices, *Science* 334 (6058) (2011) 962–965.
- [4] X. Zheng, H. Lee, T.H. Weisgraber, M. Shusteff, J. DeOtte, E.B. Duoss, J.D. Kuntz, M.M. Biener, Q. Ge, J.A. Jackson, S.O. Kucheyev, N.X. Fang, C.M. Spadaccini, Ultralight, ultrastiff mechanical metamaterials, *Science* 344 (6190) (2014) 1373–1377.
- [5] J. Bauer, S. Hengsbach, I. Tesari, R. Schwaiger, O. Kraft, High-strength cellular ceramic composites with 3D microarchitecture, *Proc. Natl. Acad. Sci. USA* 111 (7) (2014) 2453–2458.
- [6] N.A. Fleck, V.S. Deshpande, M.F. Ashby, Micro-architected materials: past, present and future, *Proc. R. Soc. A: Math. Phys. Eng. Sci.* 466 (2121) (2010) 2495–2516.
- [7] K.C. Cheung, N. Gershenfeld, Reversibly assembled cellular composite materials, *Science* 341 (6151) (2013) 1219–1221.
- [8] J. Mueller, K. Shea, Stepwise graded struts for maximizing energy absorption in lattices, *Extrem. Mech. Lett.* 25 (2018) 7–15.
- [9] S. Yuan, C.K. Chua, K. Zhou, 3D-Printed mechanical metamaterials with high energy absorption, *Adv. Mater. Technol.* 4 (3) (2019) 1–9.
- [10] Y. Gao, X. Wei, X. Han, Z. Zhou, J. Xiong, Novel 3D auxetic lattice structures developed based on the rotating rigid mechanism, *Int. J. Solids Struct.* 233 (2021).
- [11] H. Yang, L. Ma, 1D to 3D multi-stable architected materials with zero Poisson's ratio and controllable thermal expansion, *Mater. Des.* 188 (2020).
- [12] Y. Du, T. Keller, C. Song, Z. Xiao, L. Wu, J. Xiong, Design and foldability of Miura-based cylindrical origami structures, *Thin-Walled Struct.* 159 (2021), 107311.
- [13] H.N. Wadley, Multifunctional periodic cellular metals, *Philos. Trans. A Math. Phys. Eng. Sci.* 364 (2006) 31–68, 1838.
- [14] H.M.A. Kolken, S. Janbaz, S.M.A. Leeflang, K. Lietaert, H.H. Weinans, A. A. Zadpoor, Rationally designed meta-implants: a combination of auxetic and conventional meta-biomaterials, *Mater. Horiz.* 5 (1) (2018) 28–35.
- [15] T. Frenzel, C. Findeisen, M. Kadic, P. Gumbsch, M. Wegener, Tailored buckling microlattices as reusable light-weight shock absorbers, *Adv. Mater.* 28 (28) (2016) 5865.
- [16] F. Cote, R. Biagi, H. Bart-Smith, V.S. Deshpande, Structural response of pyramidal core sandwich columns, *Int. J. Solids Struct.* 44 (10) (2007) 3533–3556.
- [17] R.G. Hutchinson, N.A. Fleck, The structural performance of the periodic truss, *J. Mech. Phys. Solids* 54 (4) (2006) 756–782.
- [18] L. Dong, Mechanical response of Ti–6Al–4V hierarchical architected metamaterials, *Acta Mater.* 175 (2019) 90–106.
- [19] L. Dong, H. Wadley, Mechanical properties of carbon fiber composite octet-truss lattice structures, *Compos. Sci. Technol.* 119 (2015) 26–33.
- [20] J.C. Wallach, L.J. Gibson, Mechanical behavior of a three-dimensional truss material, *Int. J. Solids Struct.* 38 (40–41) (2001) 7181–7196.
- [21] J. Liu, Z. Zhou, L. Wu, L. Ma, Mechanical behavior and failure mechanisms of carbon fiber composite pyramidal core sandwich panel after thermal exposure, *J. Mater. Sci. Technol.* 29 (9) (2013) 846–854.
- [22] J. Liu, W. Qiao, J. Liu, D. Xie, Z. Zhou, L. Ma, L. Wu, The compressive responses of glass fiber composite pyramidal truss cores sandwich panel at different temperatures, *Compos. Part A: Appl. Sci. Manuf.* 73 (2015) 93–100.
- [23] K. Finnegan, G. Kooistra, H.N.G. Wadley, V.S. Deshpande, The compressive response of carbon fiber composite pyramidal truss sandwich cores, *Z. fuer Metal. Mater. Res. Adv. Tech.* 98 (12) (2007) 1264–1272.
- [24] W. Li, F. Sun, P. Wang, H. Fan, D. Fang, A novel carbon fiber reinforced lattice truss sandwich cylinder: fabrication and experiments, *Compos. Part A: Appl. Sci. Manuf.* 81 (2016) 313–322.
- [25] H. Fan, D. Fang, L. Chen, Z. Dai, W. Yang, Manufacturing and testing of a CFRC sandwich cylinder with Kagome cores, *Compos. Sci. Technol.* 69 (15–16) (2009) 2695–2700.
- [26] S. Jiang, F. Sun, H. Fan, D. Fang, Fabrication and testing of composite orthogrid sandwich cylinder, *Compos. Sci. Technol.* 142 (2017) 171–179.
- [27] W. Li, Q. Zheng, H. Fan, B. Ji, Fabrication and mechanical testing of ultralight folded lattice-core sandwich cylinders, *Engineering* 6 (2) (2020) 196–204.
- [28] G. Meng, B. Ji, H. Han, C. Gu, R. Lin, F. Peng, Design and simulation of an innovative cylinder fabricated by selective laser melting, *Chin. J. Aeronaut.* 32 (1) (2019) 133–142.
- [29] J. Tao, F. Li, D. Zhang, J. Liu, Z. Zhao, Manufacturing and mechanical performances of a novel foam core sandwich-walled hollow column reinforced by stiffeners, *Thin-Walled Struct.* 139 (2019) 1–8.
- [30] J. Xiong, R. Ghosh, L. Ma, A. Vaziri, Y. Wang, L. Wu, Sandwich-walled cylindrical shells with lightweight metallic lattice truss cores and carbon fiber-reinforced composite face sheets, *Compos. Part A: Appl. Sci. Manuf.* 56 (2014) 226–238.
- [31] J. Wang, W. Liu, S. Kang, T. Ma, Z. Wang, W. Yuan, H. Song, C. Huang, Compression performances and failure maps of sandwich cylinders with pyramidal truss cores obtained through geometric mapping and snap-fit method, *Compos. Struct.* 226 (2019).
- [32] M.L. Rasmussen, Waverider configurations derived from inclined circular and elliptic cones, *J. Spacecr. Rockets* 17 (6) (1980) 537–545.
- [33] L. Chen, Z. Guo, X. Deng, Z. Hou, W. Wang, Waverider configuration design with variable shock angle, *IEEE Access* 7 (2019) 42081–42093.
- [34] K.P. Zhang, Y.F. Liao, B. Qiu, Y.K. Zheng, L.K. Yu, G.H. He, Q.N. Chen, D.H. Sun, 3D printed embedded metamaterials, *Small* (2021), e2103262.
- [35] S. Babaei, J. Shim, J.C. Weaver, E.R. Chen, N. Patel, K. Bertoldi, 3D soft metamaterials with negative Poisson's ratio, *Adv. Mater.* 25 (36) (2013) 5044–5049.
- [36] N.A. Traugott, D. Mistry, C. Luo, K. Yu, Q. Ge, C.M. Yakacki, Liquid-crystal-elastomer-based dissipative structures by digital light processing 3D printing, *Adv. Mater.* 32 (28) (2020), e2000797.
- [37] S.H. Ahn, M. Montero, D. Odell, S. Roundy, P.K. Wright, Anisotropic material properties of fused deposition modeling ABS, *Rapid Prototyp. J.* 8 (4) (2002) 248–257.

- [38] Y. Xu, H. Zhang, B. Savija, S. Chaves Figueiredo, E. Schlangen, Deformation and fracture of 3D printed disordered lattice materials: Experiments and modeling, *Mater. Des.* 162 (2019) 143–153.
- [39] R. Zou, Y. Xia, S. Liu, P. Hu, W. Hou, Q. Hu, C. Shan, Isotropic and anisotropic elasticity and yielding of 3D printed material, *Compos. Part B: Eng.* 99 (2016) 506–513.
- [40] M.R. Karamooz Ravari, M. Kadkhodaei, M. Badrossamay, R. Rezaei, Numerical investigation on mechanical properties of cellular lattice structures fabricated by fused deposition modeling, *Int. J. Mech. Sci.* 88 (2014) 154–161.
- [41] R. Gautam, S. Idapalapati, S. Feih, Printing and characterisation of Kagome lattice structures by fused deposition modelling, *Mater. Des.* 137 (2018) 266–275.
- [42] W. Liu, H. Song, Z. Wang, J. Wang, C. Huang, Improving mechanical performance of fused deposition modeling lattice structures by a snap-fitting method, *Mater. Des.* 181 (2019).
- [43] W. Liu, H. Song, C. Huang, Maximizing mechanical properties and minimizing support material of PolyJet fabricated 3D lattice structures, *Addit. Manuf.* 35 (2020).
- [44] Y. Li, Q. Zhang, Y. Hong, J. Yin, 3D transformable modular kirigami based programmable metamaterials, *Adv. Funct. Mater.* (2021).
- [45] A. Bossart, D.M.J. Dykstra, J. van der Laan, C. Coulais, Oligomodal metamaterials with multifunctional mechanics, *Proc. Natl. Acad. Sci. USA* 118 (21) (2021).
- [46] B. Jenett, C. Cameron, F. Tourlomousis, A. Parra Rubio, M. Ochalek, N. Gershenfeld, Discretely assembled mechanical metamaterials, *Sci. Adv.* 6 (2020) 9943–9961.
- [47] T.G. Nelson, L.M.B. Pinto, J.T. Bruton, C.G. Nelson, L.L. Howell, Deployable convex generalized cylindrical surfaces using torsional joints, *J. Mech. Robot* 13 (2021) 1–9 (June).
- [48] M.F. Ashby, The properties of foams and lattices, *Philos. Trans. A Math. Phys. Eng. Sci.* 364 (1838) (2006) 15–30.
- [49] S.P. Timoshenko, J.M. Gere, W. Prager, *Theory of elastic stability*, second edition, *J. Appl. Mech.* 29 (1) (1962) 220–221.